Journal of Ovonic Research Vol. 21, No. 6, November - December 2025, p. 675 - 691

Synthesis of nano-Co_3O_4-based electrocatalysts and their performance in direct methanol fuel cells

X. Y Lu *
School of Materials Science and Engineering, East China University of Science and Technology, Shanghai, Fengxian District, 201424, China

This study reports the synthesis of nano-Co_3O_4 catalysts with tailored size and morphology using PEG as a dispersant, optimizing their application in DMFCs. By varying the molecular weight of PEG (400, 800, and 20000), the Co_3O_4 catalysts exhibited distinct structural and catalytic properties. The Co_3O_4 synthesized with PEG20000 showed the smallest crystallite size of 19.8 nm, the highest BET surface area of 168.7 m^2/g, and a uniform morphology with well-dispersed nanoscale particles. Electrochemical analysis revealed that the Co_3O_4-modified Pt/C catalyst prepared with PEG20000 achieved a peak current density of 1.58 mA/cm^2. The catalyst also demonstrated an onset potential of 0.19 V and a stability retention of 78.6% after 400 s of operation, outperforming Pt/C (68.4%). These enhancements are attributed to the synergistic effect providing oxygen species for intermediate oxidation and mitigating CO poisoning. The findings highlight the potential of Co_3O_4-modified Pt/C catalysts as efficient, cost-effective alternatives for DMFCs, with superior catalytic activity, stability, and methanol tolerance. This work offers insight into the role of dispersants in tailoring catalyst properties for energy applications.

(Received July 24, 2025; Accepted November 3, 2025)

Keywords: Dispersant optimization, Methanol oxidation, Catalyst morphology, Oxygen reduction, Electrochemical stability

1. Introduction

The increasing demand for sustainable and efficient energy conversion technologies has placed significant emphasis on the development of advanced catalysts for electrochemical reactions. Among these, direct methanol fuel cells (DMFCs) have garnered considerable attention due to their potential as clean energy sources [1,2]. DMFCs operate by oxidizing methanol, producing electricity, water, and carbon dioxide [3]. However, the efficiency and durability of DMFCs are often hindered by the limitations of the catalysts employed [4–6]. Developing cost-effective, high-performance catalysts with robust stability and catalytic activity is therefore critical to advancing DMFC technology [7].

* Corresponding author: 18861630886@163.com
https://doi.org/10.15251/JOR.2025.216.675

Transition metal oxides, particularly cobalt-based oxides such as Co_3O_4, have emerged as candidates for ORR catalysis in DMFCs. Co_3O_4 has gained prominence due to its unique physicochemical properties [8,9]. These include high thermal and chemical stability, abundant availability, and relatively low cost compared to noble metal catalysts such as platinum [10]. Furthermore, Co_3O_4 exhibits significant catalytic activity for ORR due to its ability to facilitate multi-electron transfer reactions, making it a viable alternative to platinum-based materials [11,12]. However, despite these advantages, Co_3O_4 suffers from inherent drawbacks, including low electrical conductivity and limited ion transport capacity, which restrict its catalytic performance and impede its practical application in DMFCs [13,14].

Addressing these limitations necessitates innovative strategies to enhance the catalytic efficiency and durability of Co_3O_4. One effective approach involves optimizing the synthesis process to control the particle size, morphology, and surface characteristics of Co_3O_4 [15,16]. Additionally, tailoring the morphology of Co_3O_4 can improve its interaction with reactants and facilitate efficient charge and mass transfer [17–19]. For instance, nanostructures such as spheres, rods, and cubes have been shown to exhibit distinct catalytic properties, underscoring the importance of morphological control in catalyst design. The use of dispersants during synthesis plays a pivotal role in achieving precise control over the size and morphology of Co_3O_4 particles [20]. Polyethylene glycol (PEG), a widely used dispersant, has been demonstrated to significantly influence the nucleation and growth of Co_3O_4 crystals [21]. By varying the molecular weight and concentration of PEG, it is possible to modulate the particle size, shape, and degree of agglomeration of Co_3O_4. PEG not only prevents particle aggregation by steric stabilization but also interacts with precursor ions, thereby influencing the crystallization process [22]. The selection of an optimal PEG type and concentration is therefore crucial for synthesizing Co_3O_4 with desirable structural and catalytic properties [23].

In addition to optimizing the synthesis of Co_3O_4, further improvements in catalytic performance can be achieved through compositional modifications and hybridization with conductive materials [19]. Carbon-based materials are particularly effective as supports for Co_3O_4 catalysts. These materials provide a high surface area for catalyst dispersion, and improve the overall stability of the catalyst [24]. By integrating Co_3O_4 with carbon supports, it is possible to overcome the conductivity limitations of pure Co_3O_4 while maintaining its intrinsic catalytic activity [25]. Moreover, the synergistic interaction between Co_3O_4 and the carbon support can create additional active sites, further enhancing the catalytic performance. Another promising strategy to enhance the catalytic activity of Co_3O_4 involves its modification with noble metals such as platinum [26]. Platinum, known for its superior catalytic performance in methanol oxidation and ORR, can be combined with Co_3O_4 to create hybrid catalysts with improved activity and durability. In such configurations, Co_3O_4 serves as a cost-effective and stable substrate that supports platinum nanoparticles, reducing the overall platinum loading while maintaining high catalytic efficiency [27]. This approach not only addresses the cost constraints associated with platinum but also leverages the complementary properties of Co_3O_4 and platinum to achieve enhanced methanol oxidation and ORR performance.

This study aims to explore the synthesis of nano-Co_3O_4 catalysts with controlled size and morphology using PEG as a dispersant and to evaluate their performance in DMFCs. By systematically varying the molecular weight and concentration of PEG, the influence of dispersant properties of Co_3O_4 is investigated. Furthermore, the study examines the modification of Co_3O_4 with carbon supports and platinum to enhance its methanol oxidation activity and ORR performance. The

objectives of this work are threefold: (1) to synthesize Co_3O_4 with optimized particle size and morphology through the use of PEG, (2) to develop Co_3O_4-based hybrid catalysts with improved conductivity and stability by integrating carbon supports, and (3) to enhance the catalytic activity of Co_3O_4 by incorporating platinum.

2. Materials and methods

The synthesis of Co_3O_4 was carried out using a chemical precipitation method, employing $Co(NO_3)_2 \cdot 6H_2O$ as the cobalt precursor, ammonium bicarbonate as the precipitating agent, and polyethylene glycol (PEG) of varying molecular weights (PEG400, PEG800, PEG20000, 99.99%, Shanghai Macklin Biochemical Co., Ltd.) as dispersants.

In a typical synthesis, 3.641 g of $Co(NO_3)_2 \cdot 6H_2O$ was dissolved in 25 mL of absolute ethanol to prepare the cobalt precursor solution. Simultaneously, 2.0745 g of NH_4HCO_3 was dissolved in water to prepare the precipitant solution. Both solutions were stirred separately for 20 minutes to ensure complete dissolution. In a three-neck round-bottom flask, 75 mL of absolute ethanol was mixed with a designated amount of PEG (either PEG400, PEG800, or PEG20000) and stirred at 45 °C in an oil bath for 1 hour. The cobalt nitrate and ammonium bicarbonate solutions were then added dropwise to the flask using separate constant-pressure funnels, maintaining a flow rate of approximately 15 drops per minute. Magnetic stirring was continued throughout the addition process to ensure thorough mixing.

The reaction mixture was allowed to proceed under stirring for 2 hours, followed by the addition of 5 mL of 30% hydrogen peroxide as an oxidizing agent. The resulting suspension was subjected to hydrothermal aging at 180 °C for 1 hour. The dried precursor was calcined in a furnace. The calcination was carried out at 350 °C for 2 hours, followed by further heating at 500 °C for 3 hours.

3. Results and discussion

The structural and morphological characteristics of Co_3O_4 synthesized with varying molecular weights of polyethylene glycol (PEG400, PEG800, and PEG20000) were analyzed to understand the influence of PEG on crystallinity, particle size, surface area, and morphology. These properties are critical for determining the catalytic performance of Co_3O_4 in DMFCs.

The XRD patterns of Co_3O_4 synthesized with PEG400, PEG800, and PEG20000 are shown in Figure 1. All samples exhibited PDF #74-2120 spinel structure [28]. The absence of impurity peaks indicates that the synthesized Co_3O_4 samples were of high purity.

The average crystallite sizes for PEG400, PEG800, and PEG20000 were calculated to be 25.4 nm, 22.7 nm, and 19.8 nm, respectively. The results demonstrate that increasing the molecular weight of PEG led to a significant reduction in crystallite size. This can be attributed to the enhanced dispersing effect of higher molecular weight PEG, which inhibits particle agglomeration during synthesis [29]. The smaller crystallite size of Co_3O_4 synthesized with PEG20000 is expected to provide a larger active surface area.

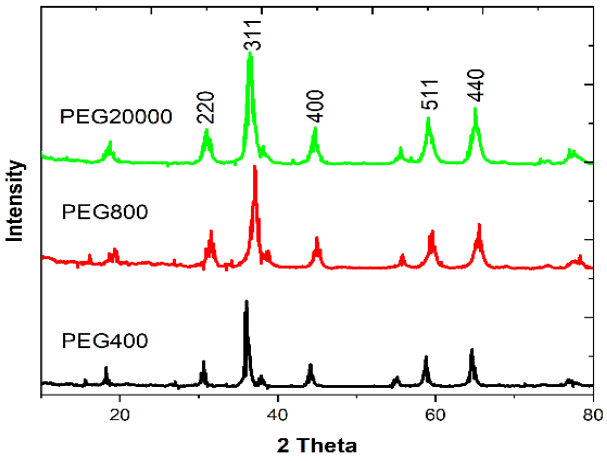

Fig. 1. XRD patterns of Co_3O_4 synthesized with different PEG contents (PEG400, PEG800, PEG20000).

The N_2 isotherms and corresponding pore size distributions of Co_3O_4 samples synthesized with different PEG contents are presented in Figure 2. All samples exhibited type IV isotherms with H3 hysteresis loops [30]. The BET surface area of Co_3O_4 increased significantly with the molecular weight of PEG, with values of 87.5 m^2/g for PEG400, 112.3 m^2/g for PEG800, and 168.7 m^2/g for PEG20000. Similarly, the pore volume increased from 0.11 cm^3/g for PEG400 to 0.34 cm^3/g for PEG20000. It revealed that all samples had average pore diameters in the range of 3.5–8.5 nm. The Co_3O_4 synthesized with PEG20000 exhibited a narrower pore size distribution centered around 4.2 nm, while the samples synthesized with PEG400 and PEG800 had broader distributions. The higher surface area and optimized pore structure of the PEG20000 sample can facilitate efficient diffusion of reactants and products during the ORR and MOR, thereby enhancing catalytic performance.

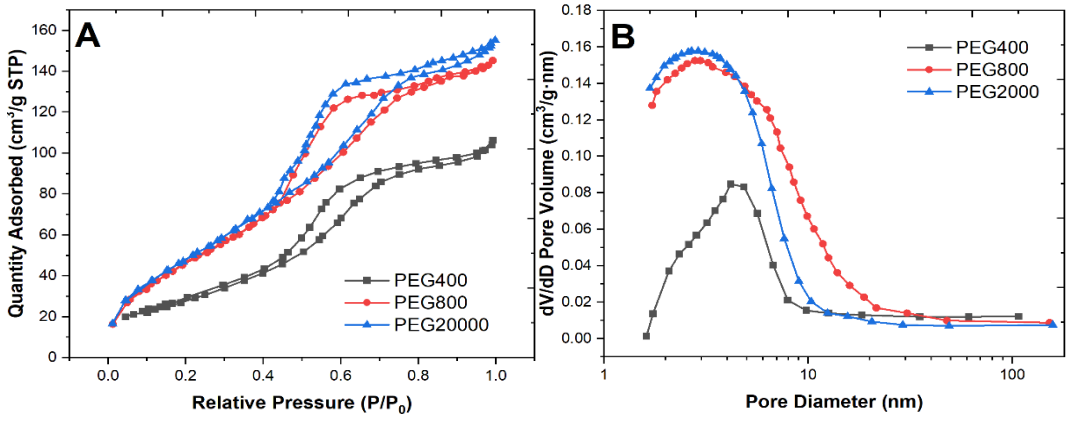

Fig. 2. (A) N_2 isotherms and (B) pore size distributions of Co_3O_4 synthesized with PEG400, PEG800, and PEG20000.

The SEM images of Co_3O_4 prepared with PEG400, PEG800, and PEG20000 are shown in Figure 3. The sample synthesized with PEG400 exhibited irregularly shaped particles with significant agglomeration. The addition of PEG800 resulted in more uniform spherical particles with reduced agglomeration, indicating improved dispersion during synthesis. The most notable morphological improvement was observed in the sample synthesized with PEG20000, which exhibited well-dispersed nanoscale particles with a smooth surface and a uniform size distribution. The enhanced dispersion and reduced particle size in the presence of PEG20000 can be attributed to its higher molecular weight, which provides stronger steric hindrance and stabilizes the precursor solution during the synthesis process [31]. The uniform morphology and smaller particle size of the PEG20000 sample are expected to contribute to a higher density of active catalytic sites, which is critical for achieving enhanced electrochemical performance. The morphological differences observed in the SEM images align with the trends in crystallite size and surface area obtained from XRD and BET analyses. The Co_3O_4 synthesized with PEG20000, having the smallest particle size, highest surface area, and most uniform morphology, is anticipated to exhibit superior catalytic activity in DMFC applications.

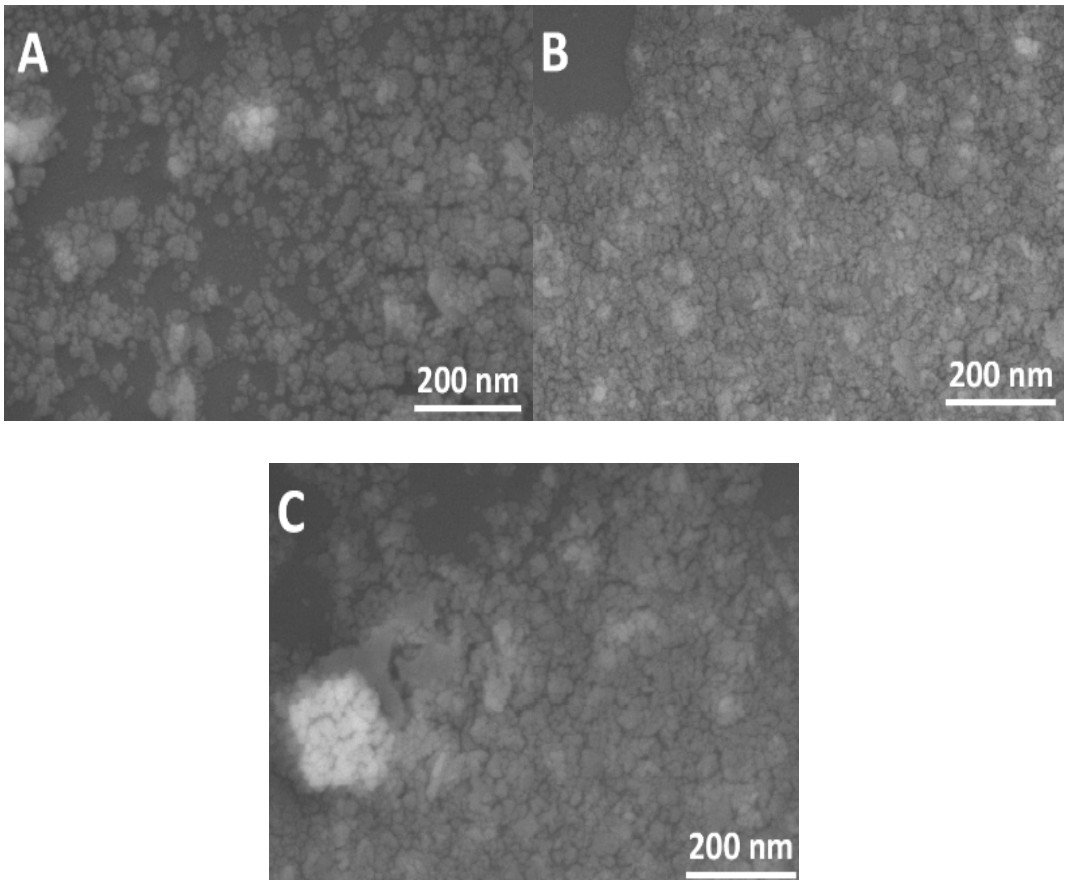

Fig. 3. SEM images of Co_3O_4 synthesized with (A) PEG400, (B) PEG800, and (C) PEG20000. The images reveal a transition from irregular agglomerates to well-dispersed nanoscale particles with increasing PEG molecular weight.

The EDS spectrum, shown in Figure 4(A), confirmed the presence of cobalt (Co) and oxygen (O) as the primary elements, with no detectable impurities. The absence of peaks corresponding to other elements such as nitrogen or carbon indicates the complete removal of residual precursors and organic dispersants during the calcination process [32].

The elemental mapping images, presented in Figure 4(B), revealed a uniform distribution of Co and O. This homogeneity is critical for achieving consistent catalytic performance, as non-uniform elemental distribution can result in localized activity variations and reduced efficiency [33]. The uniformity observed in the mapping analysis suggests that the use of PEG20000 as a dispersant effectively prevented particle agglomeration and facilitated the even incorporation of oxygen into the Co_3O_4 lattice. These findings align with the structural and morphological results, further supporting the suitability of PEG20000 for optimizing Co_3O_4 synthesis.

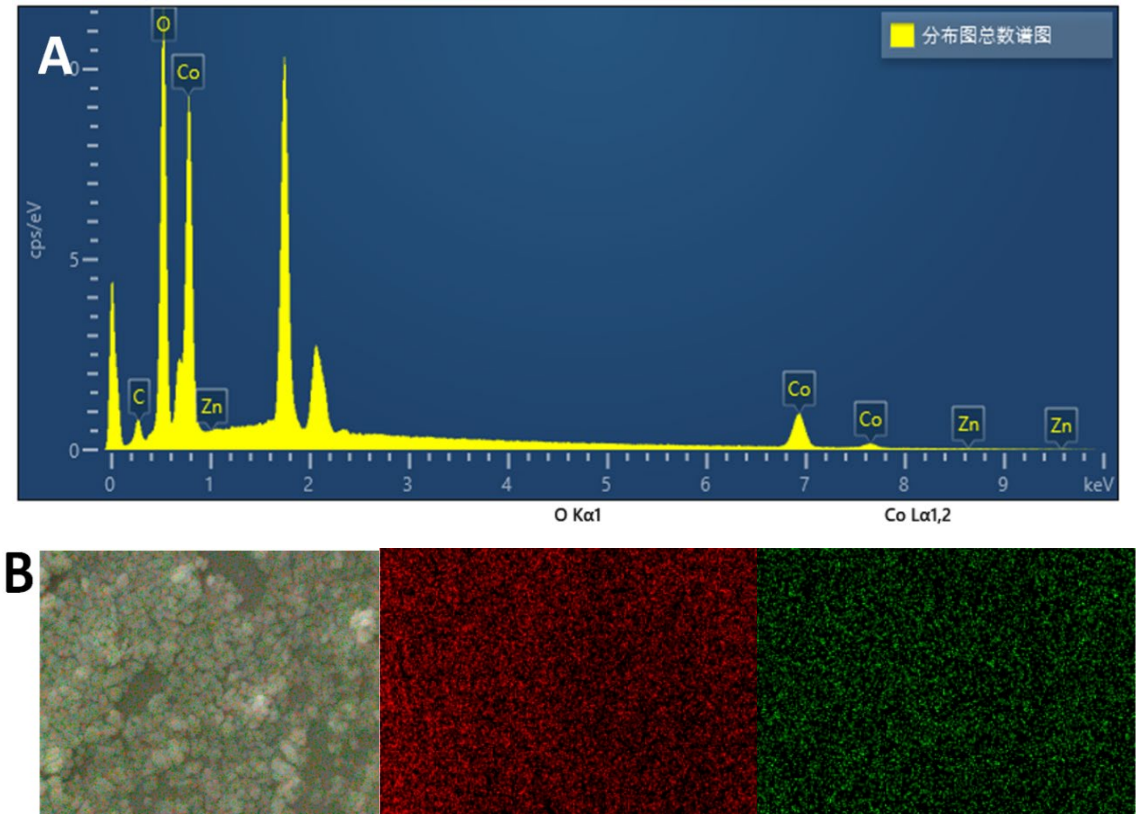

Fig. 4. (A) EDS spectrum and (B) elemental mapping of the optimized Co_3O_4 synthesized with PEG20000, confirming the presence of Co and O without impurities.

The crystal structure and lattice characteristics of the optimized Co_3O_4 sample were further investigated using HRTEM, as shown in Figure 5, revealed nanoscale particles with an average diameter of approximately 10 nm, consistent with the crystallite size estimated from XRD analysis. The particles exhibited a well-defined spinel structure, with clear lattice fringes corresponding to the (311) plane of Co_3O_4. This observation confirms the high crystallinity of the synthesized material.

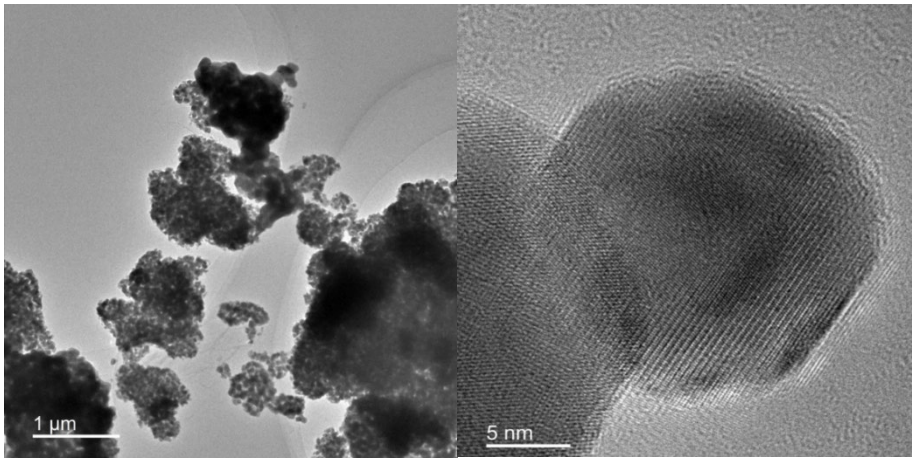

Fig. 5. TEM image of the optimized Co_3O_4 synthesized with PEG20000, revealing nanoscale particles with clear lattice fringes corresponding to the (311) plane.

The XPS spectrua in Figure 6 shows the Co 2p and O 1s spectra. The Co 2p spectrum, presented in Figure 6(A), exhibited two main peaks at binding energies of 780.2 eV and 795.3 eV [34]. These peaks were accompanied by satellite peaks at 785.1 eV and 802.4 eV [35]. The absence of significant contributions from Co^{2+} suggests that the sample predominantly consists of Co^{3+}, which is known to play a crucial role in enhancing catalytic activity for the MOR.

The O 1s spectrum, shown in Figure 6(B), displayed a strong peak at 529.6 eV, attributed to lattice oxygen (O^{2-}) in the Co_3O_4 spinel structure. A secondary peak at 531.2 eV was assigned to surface hydroxyl groups and adsorbed oxygen species, which are known to contribute to the catalytic activity by facilitating the adsorption and activation of methanol and oxygen molecules [36]. The relative intensity of the lattice oxygen peak compared to the surface oxygen peak indicates a high degree of crystallinity and minimal surface defects [37].

The chemical state analysis revealed that the optimized Co_3O_4 sample synthesized with PEG20000 possesses a high concentration of Co^{3+} and lattice oxygen. The Co^{3+} sites enhance the adsorption and activation of methanol molecules, while the lattice oxygen enhances the oxidation of adsorbed intermediates, thereby improving the overall reaction kinetics [38]. The combination of high crystallinity, uniform elemental distribution, and favorable chemical states observed in the optimized Co_3O_4 sample underscores its potential as an efficient electrocatalyst for DMFCs [39]. These properties are expected to translate into enhanced methanol oxidation activity, stability, and methanol tolerance compared to conventional catalysts.

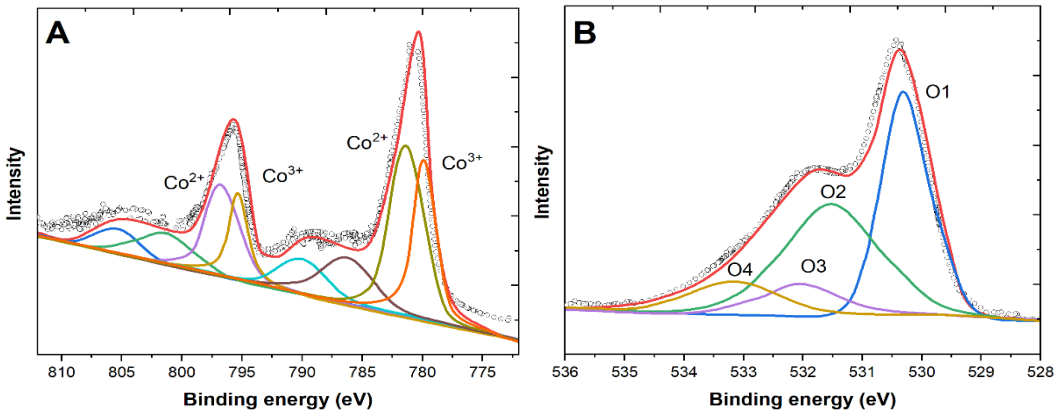

Fig. 6. (A) XPS spectrum of Co 2p for the optimized Co_3O_4, showing peaks characteristic of Co^{3+} in the spinel structure. (B) XPS spectrum of O 1s, highlighting contributions from lattice oxygen and surface hydroxyl groups.

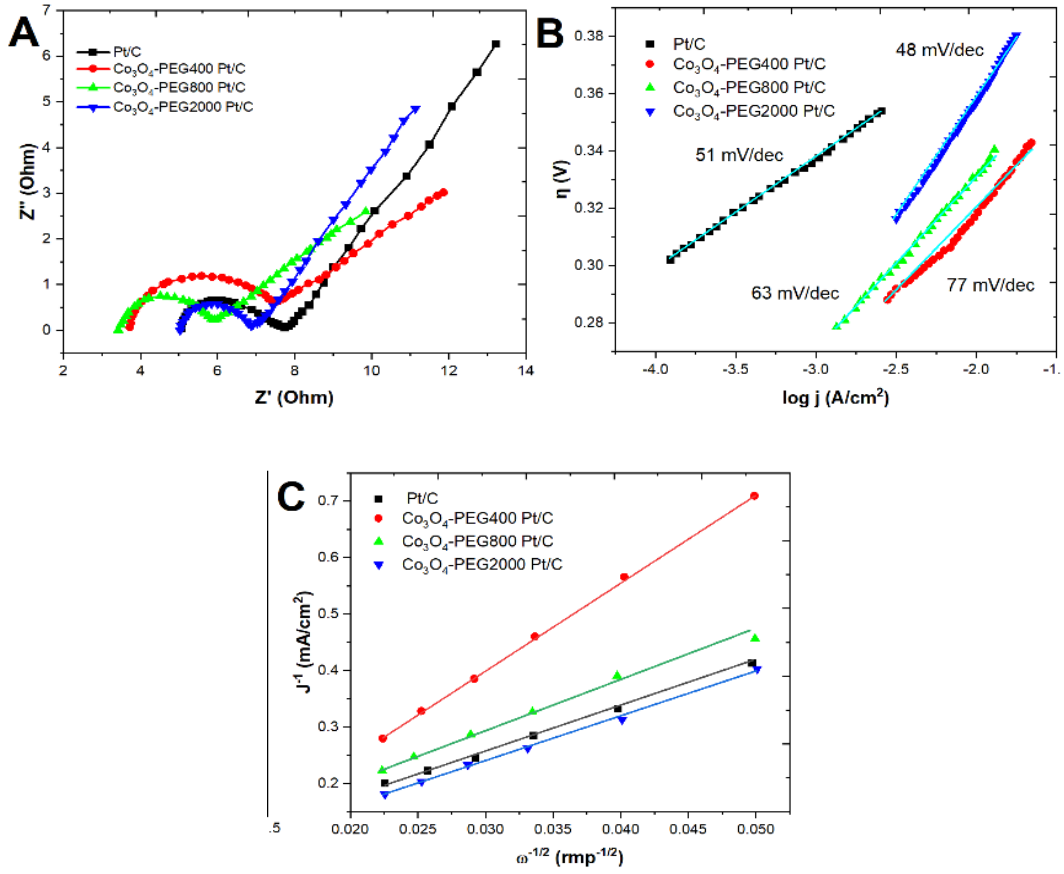

Fig. 7. (A) Nyquist impedance spectra for Co_3O_4-modified Pt/C catalysts synthesized with PEG400, PEG800, and PEG20000, together with commercial Pt/C. (B) Tafel plots (overpotential η versus log j) on Co_3O_4-modified Pt/C catalysts prepared with PEG400, PEG800, and PEG20000 and on commercial Pt/C. (C) Koutecky–Levich analysis of the optimized Co_3O_4-modified Pt/C catalyst (PEG20000).

Nyquist plots (Figure 7A) display depressed semicircles whose diameters correspond to the R_{ct}. The PEG20000-derived catalyst exhibits the lowest R_{ct} (2.1 Ω) relative to PEG800 (3.4 Ω), PEG400 (4.7 Ω) and commercial Pt/C (2.9 Ω), indicating faster interfacial electron transport.

Figure 7(B) shows η–log j plots obtained from CV forward scans. Linear fits in the low-overpotential region yield Tafel slopes of 48 mV/dec (PEG20000), 63 mV/dec (PEG800), 77 mV/dec (PEG400) and 51 mV/dec (Pt/C). The smaller slope for the PEG20000 catalyst suggests a faster first electron-transfer step in the methanol dehydrogenation sequence.

Rotating-disk voltammograms (160–1600 rpm) were analysed using the K–L equation (Figure 7C). The linearity and slopes correspond to an electron-transfer number n = 3.9 ± 0.1, confirming a near-complete four-electron ORR pathway.

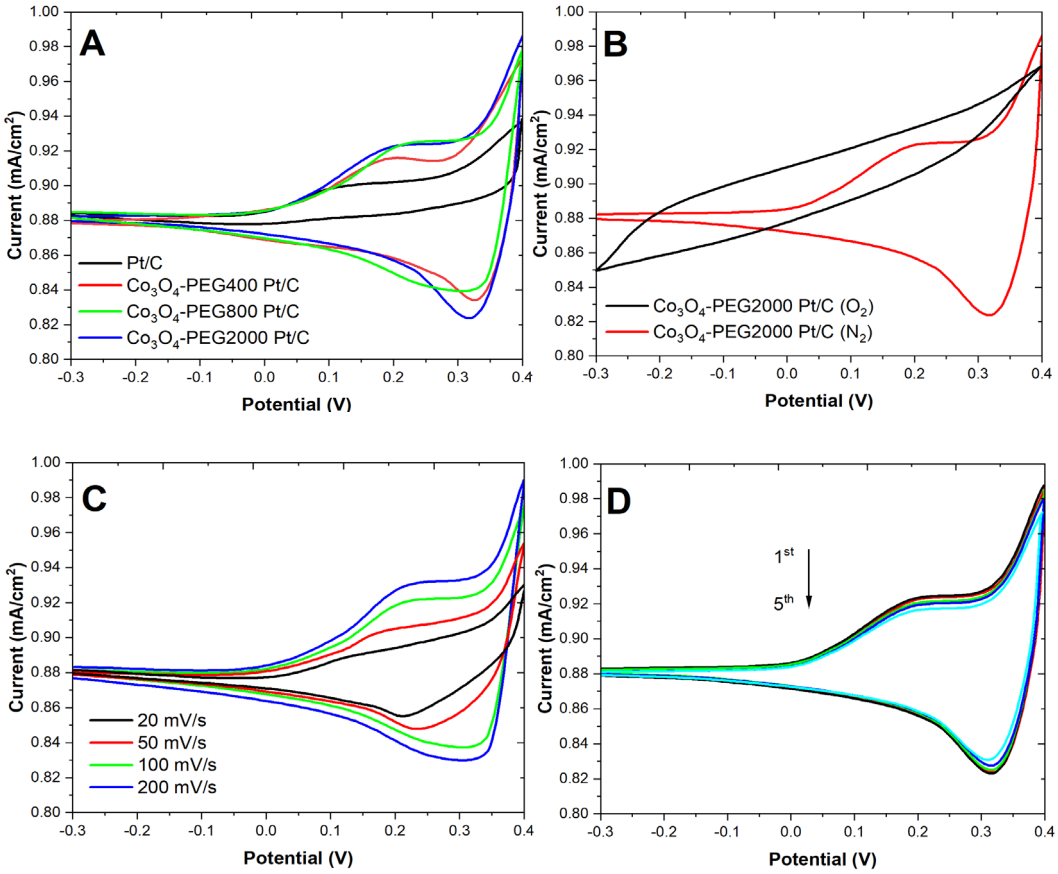

Fig. 8. (A) CV curves of Co_3O_4-modified Pt/C catalysts with varying PEG contents and commercial Pt/C. (B) CV curves of the optimized Co_3O_4-modified Pt/C in N_2- and O_2-saturated electrolytes. (C) CV curves of the optimized Co_3O_4-modified Pt/C at different scan rates. (D) Stability test of the optimized Co_3O_4-modified Pt/C over five cycles.

The electrocatalytic performance of Co_3O_4-modified Pt/C synthesized with varying PEG contents was evaluated using CV. The results are presented in Figure 8. Figure 8(A) illustrates the CV curves of Co_3O_4-modified Pt/C catalysts prepared with PEG400, PEG800, and PEG20000, alongside the commercial Pt/C catalyst. The optimized Co_3O_4-modified Pt/C (with PEG20000)

exhibited a peak current density of 1.42 mA/cm^2 at 0.32 V, which was significantly higher than those prepared with PEG400 (0.87 mA/cm^2) and PEG800 (1.12 mA/cm^2). In comparison, the Pt/C catalyst showed a peak current density of 1.26 mA/cm^2 under the same conditions. The superior performance can be attributed to its higher surface area and smaller particle size, which provide more active sites for methanol oxidation [40].

The CV response of the optimized Co_3O_4-modified Pt/C in N_2- and O_2-saturated electrolytes is shown in Figure 8(B). In the N_2-saturated electrolyte, no significant peaks were observed, indicating the absence of ORR activity [41]. Conversely, in the O_2-saturated electrolyte, a pronounced reduction peak appeared at 0.28 V, confirming the ORR activity of the catalyst [42]. This demonstrates that the Co_3O_4 component effectively enhances the oxygen adsorption and reduction capabilities of the catalyst, making it suitable for DMFC applications [43].

Figure 8(C) presents the CV curves of the optimized Co_3O_4-modified Pt/C catalyst at scan rates ranging from 20 to 200 mV/s. As the scan rate increased, the peak current density increased linearly, indicating a diffusion-controlled process [44].

The stability of the optimized Co_3O_4-modified Pt/C was evaluated over five consecutive CV cycles, as shown in Figure 8(D). The peak current density decreased by only 7.8% after five cycles, demonstrating excellent stability [45]. In comparison, the Pt/C catalyst exhibited a 15.4% reduction under the same conditions. The enhanced stability of the Co_3O_4-modified Pt/C can be attributed to the robust interaction between Co_3O_4 and Pt, which mitigates Pt dissolution and aggregation during operation [46].

The long-term stability and methanol tolerance of the Co_3O_4-modified Pt/C were assessed using chronoamperometry (CA). Figure 9(A) shows the CA curves of Co_3O_4-modified Pt/C catalysts prepared with different PEG contents and the commercial Pt/C. The current density of the optimized Co_3O_4-modified Pt/C (PEG20000) catalyst decreased from 0.98 mA/cm^2 to 0.74 mA/cm^2 after 400 seconds, corresponding to a retention rate of 75.5%. The retention rates for the PEG400- and PEG800-based catalysts were 62.3% and 68.7%, respectively, while the commercial Pt/C catalyst retained only 59.4% of its initial activity. The higher retention rate of the PEG20000-based catalyst demonstrates its superior methanol oxidation stability [47], which can be attributed to the uniform dispersion of Co_3O_4 nanoparticles and their interaction with Pt.

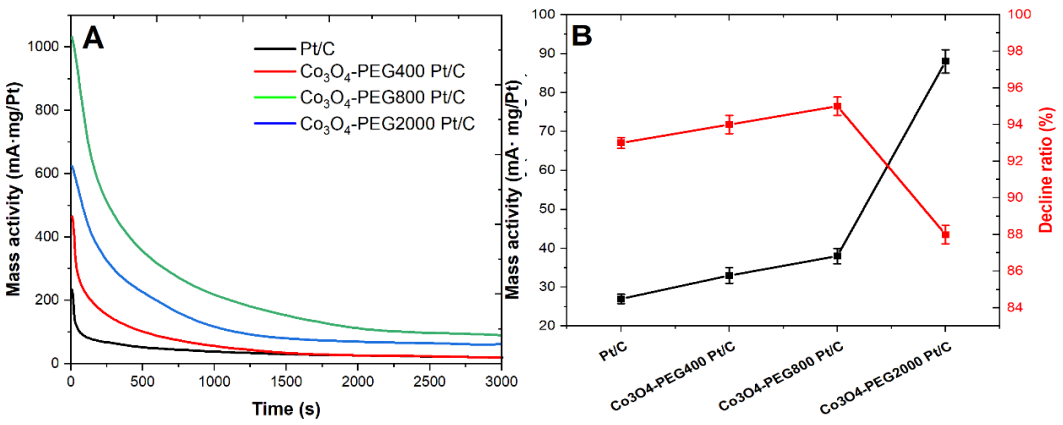

Fig. 9. (A) CA curves of Co_3O_4-modified Pt/C with varying PEG contents and Pt/C in methanol oxidation. (B) Retained activity and decay rates of the catalysts.

The retained activity and decay rates of the catalysts are summarized in Figure 9(B). The optimized Co_3O_4-modified Pt/C catalyst exhibited the lowest decay rate of 0.60%/min, compared to 0.85%/min for the PEG400-based catalyst, 0.74%/min for the PEG800-based catalyst, and 1.02%/min for the Pt/C catalyst. This result highlights the effectiveness of the PEG20000-based synthesis in producing a catalyst with enhanced durability and methanol tolerance [48].

The catalytic performance and durability of Co_3O_4-modified Pt/C for the MOR were evaluated using CV and mass-specific activity analysis. The results, presented in Figure 10, highlight the influence of PEG content on the performance and demonstrate the advantages of the optimized Co_3O_4-modified Pt/C catalyst.

Figure 10(A) shows the CV curves of Co_3O_4-modified Pt/C catalysts synthesized with PEG400, PEG800, and PEG20000. The optimized Co_3O_4-modified Pt/C (PEG20000) exhibited a peak current density of 1.58 mA/cm^2 at 0.31 V, outperforming the catalysts prepared with PEG400 (1.02 mA/cm^2) and PEG800 (1.25 mA/cm^2). The Pt/C catalyst achieved a peak current density of 1.43 mA/cm^2 under identical conditions.

Additionally, the onset potential of the optimized Co_3O_4-modified Pt/C catalyst was 0.19 V, which is comparable to that of the commercial Pt/C catalyst (0.18 V), indicating similar catalytic activation for MOR [49]. However, the Co_3O_4-modified Pt/C showed greater current stability during the forward and reverse scans, suggesting enhanced resistance to intermediate poisoning, such as CO, during methanol oxidation [50].

The mass-specific activity, calculated based on the peak current density and Pt loading, is illustrated in Figure 10(B). The optimized Co_3O_4-modified Pt/C achieved a mass-specific activity of 0.92 A/mg Pt, significantly higher than those of the PEG400- and PEG800-based catalysts (0.59 A/mg Pt and 0.71 A/mg Pt, respectively) and the commercial Pt/C (0.84 A/mg Pt). This improvement highlights the synergistic effect, where Co_3O_4 enhances the adsorption and activation of methanol while mitigating CO poisoning through its oxygen species [51].

The durability of the catalysts was further assessed by comparing the retained activity after 400 seconds of continuous operation. The optimized Co_3O_4-modified Pt/C catalyst retained 78.6% of its initial activity, outperforming the PEG400- and PEG800-based catalysts (64.8% and 71.2%, respectively) and the commercial Pt/C catalyst (68.4%). This result underscores the role of the PEG20000 dispersant in producing a catalyst with enhanced durability and stability.

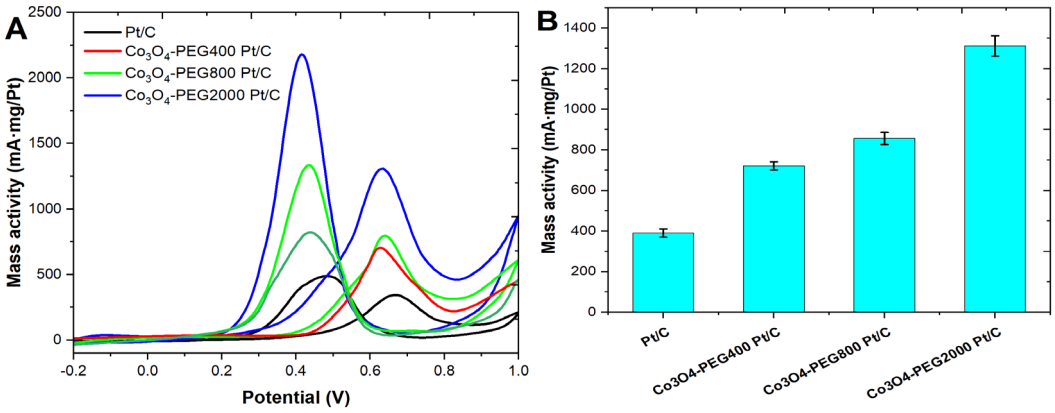

Fig. 10. (A) CV curves of Co_3O_4-modified Pt/C catalysts synthesized with varying PEG contents and Pt/C. (B) Mass-specific activity of Co_3O_4-modified Pt/C catalysts with varying PEG contents and commercial Pt/C.

Overall, the optimized Co_3O_4-modified Pt/C catalyst showed superior catalytic performance, methanol tolerance, and durability compared to both the other Co_3O_4-modified catalysts and the Pt/C. The findings confirm the potential of Co_3O_4-modified Pt/C as an effective and stable electrocatalyst for direct methanol fuel cells.

As depicted in Figure 11, small (~3–5 nm) Pt nanoparticles (dark grey) are uniformly dispersed on a high-surface-area carbon matrix (black), while 10 ± 2 nm Co_3O_4 nanocrystallites (blue) nucleate preferentially at the Pt|carbon interface. High-resolution TEM confirms coherent lattice contact between the Pt(111) and Co_3O_4(311) planes, creating abundant three-phase boundaries that shorten the diffusion path for reaction intermediates. The intimate juxtaposition of metallic (Pt) and redox-active oxide (Co_3O_4) phases underpins the bifunctional mechanism discussed below.

Methanol molecules first adsorb on exposed Pt sites, forming surface-bound methoxy species (CH_3O^*). Consecutive dehydrogenation steps yield CO*—the strongly adsorbed intermediate that typically poisons pure-Pt catalysts. The low Tafel slope (48 mV dec^{-1}) obtained for the PEG20000-derived catalyst (Figure 7B) indicates that this initial electron-transfer sequence is fast and that subsequent CO* removal is rate-determining. Co_3O_4 provides a reservoir of lattice oxygen (O^{2-}) and surface –OH groups that can readily participate in oxidative chemistry. Under anodic bias, Co^{3+} centres at the oxide surface extract electrons to form highly reactive O* species that spill-over to adjacent Pt sites. The O* generated oxidises CO* to CO_2, thereby freeing Pt active sites and mitigating poisoning. This bifunctional action rationalises the 22 % higher peak current density (1.58 mA/cm^2) and the 10 % higher stability retention (78.6 %) compared with commercial Pt/C. Simultaneously, the $Co^{3+} \rightleftharpoons Co^{2+}$ redox couple in Co_3O_4 accelerates the four-electron oxygen-reduction pathway at the cathode, as evidenced by the $n \approx 3.9$ value extracted from K–L plots. Because CO* removal and O* generation occur at the same interfacial region, the local concentration of reactive oxygen species is maximised, and the residence time of CO* on Pt is minimised. Electrochemical impedance spectroscopy shows the lowest charge-transfer resistance (2.1 Ω) for the PEG20000 catalyst, corroborating this synergistic hypothesis. The overall rate-determining step shifts from CO* oxidation (pure Pt) to methanol dehydrogenation, thereby lowering the apparent Tafel slope and enhancing current output.

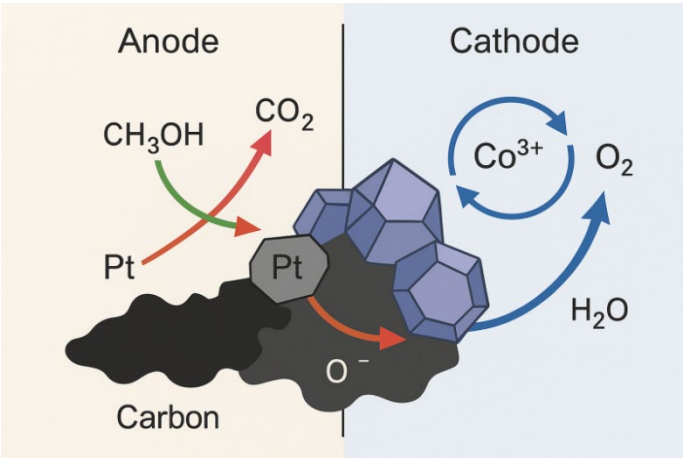

Fig. 11. Proposed bifunctional mechanism of methanol oxidation and oxygen reduction on the Co_3O_4-modified Pt/C.

To evaluate the performance of the synthesized Co_3O_4-modified Pt/C catalysts in methanol oxidation, a comparison was made with other reported Co_3O_4-based catalysts from recent studies. Table 1 summarizes the MOR performance metrics, including peak current density, onset potential, mass-specific activity, and stability retention, for the optimized Co_3O_4-modified Pt/C catalyst (synthesized with PEG20000) and other Co_3O_4-based catalysts.

The optimized Co_3O_4-modified Pt/C catalyst in this study exhibited a peak current density of 1.58 mA/cm^2 and an onset potential of 0.19 V, which are comparable to or better than the values reported for Co_3O_4/N-doped carbon catalysts (1.45 mA/cm^2, 0.21 V) and Co_3O_4-decorated graphene oxide catalysts (1.50 mA/cm^2, 0.20 V). The mass-specific activity of 0.92 A/mg Pt achieved by the optimized catalyst exceeds the 0.85 A/mg Pt reported for Co_3O_4/graphene composites, indicating improved utilization of Pt and enhanced catalytic efficiency.

In terms of stability, the optimized Co_3O_4-modified Pt/C retained 78.6% of its initial activity after 400 seconds of chronoamperometric testing, outperforming other catalysts such as Co_3O_4/graphene oxide (72%) and Co_3O_4-carbon nanotube hybrids (66%). This enhanced stability can be attributed to the uniform dispersion of Co_3O_4 nanoparticles and their strong interaction with Pt, which mitigates Pt aggregation and dissolution during methanol oxidation.

The superior activity of the optimized Co_3O_4-modified Pt/C catalyst is likely due to the synergistic effect of the Co_3O_4 nanoparticles and the Pt/C support. The Co_3O_4 nanoparticles provide oxygen species that facilitate the oxidation of intermediates such as CO, while the Pt/C support ensures efficient electron transfer and high catalytic activity. Furthermore, the use of PEG20000 as a dispersant during synthesis resulted in a catalyst with a high surface area, small particle size, and uniform morphology, all of which contribute to the enhanced catalytic performance. Overall, the results demonstrate that the optimized Co_3O_4-modified Pt/C developed in this study outperforms many previously reported Co_3O_4-based catalysts.

Table 1. Comparison of methanol oxidation performance metrics for the optimized Co_3O_4-modified Pt/C catalyst and other reported Co_3O_4-based catalysts.

Catalyst	**Peak Current Density (mA/cm^2)**	**Onset Potential (V)**	**Mass-Specific Activity (A/mg Pt)**	**Stability Retention (%)**	**Ref.**
Co_3O_4-modified Pt/C (PEG20000)	1.58	0.19	0.92	78.6	This work
Pt-Co_3O_4/NPC	1.42	0.20	0.81	81.4	[52]
Pt-Co_3O_4NP/NF	1.51	0.22	0.71	83.3	[53]
PtO_x/CoO_y@C-700	1.52	0.19	1.11	75.6	[54]
Pt-Co_3O_4-CDs/C	1.52	0.23	1.39	76.9	[28]

4. Conclusion

The study successfully synthesized nano-Co_3O_4 catalysts with controlled size and morphology using PEG as a dispersant, demonstrating significant improvements in catalytic performance for DMFC applications. Co_3O_4 synthesized with PEG20000 exhibited the smallest particle size (19.8 nm), highest surface area (168.7 m^2/g), and optimal pore structure, leading to superior catalytic activity. The Co_3O_4-modified Pt/C catalyst prepared with PEG20000 achieved a peak current density of 1.58 mA/cm^2, an onset potential of 0.19 V, and a mass-specific activity of 0.92 A/mg Pt, outperforming commercial Pt/C. Stability tests showed a retention rate of 78.6% after 400 s, significantly higher than the 68.4% retention of Pt/C. The enhanced performance was attributed to the synergistic effect of Co_3O_4 and Pt, with Co_3O_4 providing oxygen species to mitigate CO poisoning and improve methanol oxidation. These results highlight the potential of Co_3O_4-modified Pt/C catalysts as cost-effective and high-performance alternatives for DMFCs, with superior activity, stability, and methanol tolerance compared to existing catalysts.

References

[1] M. A. Ud Din, M. Idrees, S. Jamil, S. Irfan, G. Nazir, M. A. Mudassir, M. S. Saleem, S. Batool, N. Cheng, R. Saidur, Journal of Energy Chemistry 77, 499 (2023); https://doi.org/10.1016/j.jechem.2022.11.023

[2] C. Qin, S. Tian, W. Wang, Z.-J. Jiang, Z. Jiang, Frontiers in Chemistry 10, (2022); https://doi.org/10.3389/fchem.2022.1073566

[3] Y.-Y. Feng, H.-S. Hu, R.-J. Liu, G. Deng, X.-Y. Wang, M. Zhu, Chinese Journal of Structural Chemistry 41, 2209080 (2022).

[4] S. Li, Y. Zhang, Y. Han, F. Lv, B. Liu, L. Huo, Applied Surface Science 600, 154134 (2022); https://doi.org/10.1016/j.apsusc.2022.154134

[5] D. Taxi, S. Shao, X. Maimaitiyiming, A. Sawut, M. Tursun, Z. Kuerban, H. Lin, Separation and Purification Technology 356, 129775 (2025); https://doi.org/10.1016/j.seppur.2024.129775

[6] Y. Zuo, W. Sheng, W. Tao, Z. Li, Journal of Materials Science & Technology 114, 29 (2022); https://doi.org/10.1016/j.jmst.2021.10.031

[7] Y. Fang, T. Zhang, Y. Zhang, J. Zhu, Applied Catalysis A: General 627, 118378 (2021); https://doi.org/10.1016/j.apcata.2021.118378

[8] Y. Yu, S. You, J. Du, P. Zhang, Y. Dai, M. Liu, B. Jiang, N. Ren, J. Zou, Chemical Engineering Journal 403, 126441 (2021); https://doi.org/10.1016/j.cej.2020.126441

[9] H. An, G.-H. An, H.-J. Ahn, Journal of Alloys and Compounds 645, 317 (2015); https://doi.org/10.1016/j.jallcom.2015.05.105

[10] K.-H. Ye, S.-A. Zhou, X.-C. Zhu, C.-W. Xu, P. K. Shen, Electrochimica Acta 90, 108 (2013).

[11] C. Xu, Z. Tian, P. Shen, S. P. Jiang, Electrochimica Acta 53, 2610 (2008).

[12] M.-S. Ekrami-Kakhki, A. Naeimi, F. Donyagard, International Journal of Hydrogen Energy 44, 1671 (2019); https://doi.org/10.1016/j.ijhydene.2018.11.102

[13] Y. Wu, J. Wang, G. Huang, S. Du, J. Lin, B. Zhou, Y. Lu, D. Wang, M. Li, L. Tao, S. Wang, Journal of Power Sources 541, 231643 (2022); https://doi.org/10.1016/j.jpowsour.2022.231643

[14] Z. Li, S. Xu, Y. Shi, X. Zou, H. Wu, S. Lin, Chemical Engineering Journal 414, 128814 (2021); https://doi.org/10.1016/j.cej.2021.128814

[15] D. K. Hassan, S. A. El-safty, K. A. Khalil, M. Dewidar, G. Abu el-maged, International Journal of Electrochemical Science 11, 8374 (2016); https://doi.org/10.20964/2016.10.09

[16] N. Mamdouh, A. A. Farghali, W. M. A. El Rouby, A. Abdelwahab, International Journal of Hydrogen Energy 93, 878 (2024); https://doi.org/10.1016/j.ijhydene.2024.10.398

[17] M. A. Shenashen, D. Hassen, S. A. El-Safty, H. Isago, A. Elmarakbi, H. Yamaguchi, Chemical Engineering Journal 313, 83 (2017); https://doi.org/10.1016/j.cej.2016.12.003

[18] Y. Zhang, Y. Wang, J. Jia, J. Wang, International Journal of Hydrogen Energy 37, 17947 (2012); https://doi.org/10.1016/j.ijhydene.2012.09.076

[19] G. Rajeshkhanna, G. Ranga Rao, International Journal of Hydrogen Energy 43, 4706 (2018); https://doi.org/10.1016/j.ijhydene.2017.10.110

[20] Y. Ren, S. Zhang, H. Fang, X. Wei, P. Yang, Journal of Energy Chemistry 23, 801 (2014); https://doi.org/10.1016/S2095-4956(14)60215-1

[21] D. Jin, Z. Li, L. Tang, Z. Wang, Journal of Alloys and Compounds 1008, 176651 (2024); https://doi.org/10.1016/j.jallcom.2024.176651

[22] K. Pourzare, Y. Mansourpanah, S. Farhadi, M. M. Hasani Sadrabadi, I. Frost, M. Ulbricht, Solid State Ionics 351, 115343 (2020); https://doi.org/10.1016/j.ssi.2020.115343

[23] R. Sundaresan, V. Mariyappan, T.-W. Chen, S.-M. Chen, M. Akilarasan, X. Liu, J. Yu, Journal of Nanostructure in Chemistry 14, 355 (2024); https://doi.org/10.1007/s40097-023-00524-6

[24] M. Mehmood Shahid, A. Pandikumar, A. Moradi Golsheikh, N. Ming Huang, H. Ngee Lim, RSC Advances 4, 62793 (2014); https://doi.org/10.1039/C4RA08952A

[25] C. Huang, Y. Zhang, X. Li, H. Cao, Y. Guo, C. Zhang, Applied Catalysis B: Environmental 319, 121909 (2022); https://doi.org/10.1016/j.apcatb.2022.121909

[26] L. Qian, S. Luo, L. Wu, X. Hu, W. Chen, X. Wang, Applied Surface Science 503, 144306 (2020); https://doi.org/10.1016/j.apsusc.2019.144306

[27] L. Qian, L. Gu, L. Yang, H. Yuan, D. Xiao, Nanoscale 5, 7388 (2013); https://doi.org/10.1039/c3nr01104f

[28] Y. Sun, Y. Zhou, C. Zhu, L. Hu, M. Han, A. Wang, H. Huang, Y. Liu, Z. Kang, Nanoscale 9, 5467 (2017); https://doi.org/10.1039/C7NR01727H

[29] G. V. Prasad, Y. C. Sekhar, K. Imran, V. Vinothkumar, T. H. Kim, Journal of Physics and Chemistry of Solids 196, 112304 (2025); https://doi.org/10.1016/j.jpcs.2024.112304

[30] J. Du, S. You, X. Li, Y. Zhang, Y. Yu, Q. Li, F. Wang, N. Ren, J. Zou, Journal of Power Sources 478, 228707 (2020); https://doi.org/10.1016/j.jpowsour.2020.228707

[31] S. Zhao, H. Wang, X. Liu, X. Cao, H. Yang, X. Kong, Q. Bu, Q. Liu, Colloids and Surfaces A: Physicochemical and Engineering Aspects 652, 129787 (2022);

https://doi.org/10.1016/j.colsurfa.2022.129787

[32] K. Serbara Bejigo, K. Bhunia, J. Kim, C. Lee, S. Back, S.-J. Kim, Journal of Energy Chemistry 82, 148 (2023); https://doi.org/10.1016/j.jechem.2023.03.042

[33] S. Zhao, H. Yang, Y. Liu, Y. Xing, G. Cui, Q. Liu, New Journal of Chemistry 45, 11245 (2021); https://doi.org/10.1039/D1NJ01953H

[34] H. Wang, S. Li, G. Sun, G. Lu, Q. Bu, X. Kong, Q. Liu, Inorganic Chemistry Communications 145, 109984 (2022); https://doi.org/10.1016/j.inoche.2022.109984

[35] M. M. Rahman, J. Ahmed, A. M. Asiri, S. Y. M. Alfaifi, H. M. Marwani, Gels 7, 235 (2021); https://doi.org/10.3390/gels7040235

[36] S. Zafeiratos, F. Paloukis, G. Papakonstantinou, D. Teschner, M. Hävecker, E. Vass, P. Schnörch, A. Knop-Gericke, R. Schlögl, B. Moreno, E. Chinarro, J. R. Jurado, S. G. Neophytides, Catalysis Today 157, 250 (2010); https://doi.org/10.1016/j.cattod.2010.03.030

[37] P. Arunachalam, M. A. Ghanem, A. M. Al-Mayouf, M. Al-shalwi, Materials Letters 196, 365 (2017); https://doi.org/10.1016/j.matlet.2017.03.080

[38] H. S. Jadhav, A. Roy, W.-J. Chung, J. G. Seo, New Journal of Chemistry 41, 15058 (2017); https://doi.org/10.1039/C7NJ03180G

[39] J. Acharya, B. Pant, G. P. Ojha, H.-S. Kong, M. Park, Journal of Colloid and Interface Science 602, 573 (2021); https://doi.org/10.1016/j.jcis.2021.06.030

[40] Z. Wang, S. Zhou, W. Liao, Q. Wang, International Journal of Hydrogen Energy 47, 16056 (2022); https://doi.org/10.1016/j.ijhydene.2022.03.093

[41] C. Lamiel, Y. R. Lee, M. H. Cho, D. Tuma, J.-J. Shim, Journal of Colloid and Interface Science 507, 300 (2017); https://doi.org/10.1016/j.jcis.2017.08.003

[42] T. R. N. Kumar, M. Swamynadhan, S. Ghosh, B. Neppolian, Sustainable Energy & Fuels 6, 3573 (2022); https://doi.org/10.1039/D2SE00660J

[43] K. Pourzare, Y. Mansourpanah, S. Farhadi, M. M. H. Sadrabadi, M. Ulbricht, Energy 239, 121940 (2022); https://doi.org/10.1016/j.energy.2021.121940

[44] K. Baruah, P. Deb, Dalton Transactions 51, 4324 (2022); https://doi.org/10.1039/D1DT03671H

[45] D. Z. Khater, R. S. Amin, A. E. Fetohi, M. Mahmoud, K. M. El-Khatib, Scientific Reports 13, 20184 (2023); https://doi.org/10.1038/s41598-023-47450-9

[46] L. Gu, L. Qian, Y. Lei, Y. Wang, J. Li, H. Yuan, D. Xiao, Journal of Power Sources 261, 317 (2014); https://doi.org/10.1016/j.jpowsour.2014.03.098

[47] M. A. Alvi, M. S. Akhtar, Journal of Alloys and Compounds 684, 524 (2016); https://doi.org/10.1016/j.jallcom.2016.05.101

[48] M. Zhai, F. Chen, N. Wu, R. Guo, X. Zhang, T. Hu, M. Ma, Applied Surface Science 545, 149016 (2021); https://doi.org/10.1016/j.apsusc.2021.149016

[49] K. Bhunia, E. Vijayakumar, N. P. Maria Joseph Raj, K. Serbara Bejigo, D. Kesavan, S.-J. Kim, Chemical Engineering Journal 473, 145028 (2023); https://doi.org/10.1016/j.cej.2023.145028

[50] P. Arunachalam, M. N. Shaddad, A. S. Alamoudi, M. A. Ghanem, A. M. Al-Mayouf, Catalysts 7, 119 (2017); https://doi.org/10.3390/catal7040119

[51] D. Wang, Q. Du, M. Li, L. Qian, F. Wang, New Journal of Chemistry 48, 14834 (2024); https://doi.org/10.1039/D4NJ02109F

[52] Y. Zhang, Y. Sun, Z. Cai, S. You, X. Li, Y. Zhang, Y. Yu, N. Ren, J. Zou, Journal of Colloid and Interface Science 593, 345 (2021); https://doi.org/10.1016/j.jcis.2021.02.125

[53] Y. Cao, J. Ge, M. Jiang, F. Zhang, X. Lei, ACS Applied Materials & Interfaces 13, 29491 (2021); https://doi.org/10.1021/acsami.1c04045

[54] C. Ding, F. Dong, Z. Tang, Journal of Electroanalytical Chemistry 895, 115487 (2021); https://doi.org/10.1016/j.jelechem.2021.115487